Green Chemistry

PAPER

View Article Online
View Journal | View Issue

Cite this: *Green Chem.*, 2024, **26**, 8267

Non-noble metal heterogeneous catalysts for hydrogen-driven deoxydehydration of vicinal diol compounds†

Jianxing Gan, [a] Yoshinao Nakagawa, *[a,b] Mizuho Yabushita [a,b] and Keiichi Tomishige *[a,b,c]

Noble-metal-free heterogeneous catalysts for deoxydehydration (DODH) using H_2 as a reductant were developed. Among various transition metals examined as additives to modify the MoO_x/TiO_2 catalyst, Cu showed good conversion and selectivity in the transformation of 1,4-anhydroerythritol (1,4-AHERY) to 2,5-dihydrofuran (2,5-DHF). The performance of the MoO_x–Cu/TiO_2 catalysts was comparable to those modified with either Ag or Au instead of Cu. Upon the combination of two Mo precursors, *i.e.* $(NH_4)_6Mo_7O_{24}$ and Na_2MoO_4, the selectivity of the catalyst (MoO_x–Cu–Na/TiO_2) was further enhanced to achieve 81% yield of 2,5-DHF. This catalyst also exhibited broad substrate scope including cyclic and linear alkyl vicinal diols and tartaric ester. Furthermore, MoO_x–Cu–Na/TiO_2 was reusable at least three times after its calcination as regeneration. The reaction was almost zero-order with respect to the H_2 pressure and 1,4-AHERY concentration, suggesting that the release of the alkene is the rate-determining step. The comprehensive characterization using STEM, XRD and XAFS provided insights into the surface structure of the catalyst, revealing that H_2 is activated over Cu particles and subsequently transferred to Mo cluster species on the TiO_2 surface *via* the spillover effect to proceed with the DODH reaction.

Received 23rd April 2024,
Accepted 7th June 2024

DOI: 10.1039/d4gc02006e

rsc.li/greenchem

Introduction

The depletion of fossil resources, coupled with rising mining costs, requires the establishment of an alternative means of supplying chemicals from sustainable feedstock such as biomass.[1–3] Although a variety of processes for biomass conversion into chemicals have been established thus far,[4–8] most processes are still under development. For example, olefinic compounds are essential platform chemicals because they can be derivatized into various products. Olefinic compounds have been manufactured on an industrial scale from petroleum *via* cracking reactions, while their production from biomass is difficult due to the high oxygen content in biomass-derived compounds. The development of catalytic systems capable of converting oxygen-rich biomass-derived compounds into alkenes and unsaturated oxygenates is, therefore, considered as the hot topic in the field of biorefinery.[9–11]

The deoxydehydration (DODH) reaction converts vicinal OH groups to the C=C bond and is promising as a selective approach to converting biomass to olefinic compounds.[12–14] The catalysts for DODH are mainly homogeneous Re complexes such as methyltrioxorhenium.[15–17] DODH with such Re catalysts proceeds *via* the two-electron redox cycle of the high-valent metal center (Re^{VII} and Re^{V}). The catalytic DODH systems developed earlier used expensive and environmentally unfriendly reductants such as triphenylphosphine (PPh_3),[18,19] sodium sulfite (Na_2SO_3)[20] and secondary alcohols.[21–23] Molecular hydrogen (H_2) is an inexpensive and green reductant in industry and generally used in the reductive conversion of biomass into chemicals and fuels such as hydrogenated vegetable oil.[24–28] However, the use of H_2 in homogeneous catalysts is difficult because H_2 is hardly activated by homogeneous catalysts, making H_2-driven DODH systems uncommon.[29,30]

Heterogeneous Re catalysts for DODH have been recently developed, and the combination of ReO_x/CeO_2 and a metal promoter is effective for H_2-driven DODH reactions. In this system, a metal promoter activates H_2 to help the reduction step of the Re center in the catalytic DODH cycle. Some catalysts give saturated di-deoxygenated products instead of alkenes because such a metal promotor can also catalyze the

[a]*Department of Applied Chemistry, School of Engineering, Tohoku University, 6-6-07 Aoba, Aramaki, Aoba-ku, Sendai, 980-8579, Japan. E-mail: yoshinao@erec.che.tohoku.ac.jp, tomishige@tohoku.ac.jp; Tel: +81-22-752-2223, +81-22-795-7214*
[b]*Research Center for Rare Metal and Green Innovation, Tohoku University, 468-1 Aoba, Aramaki, Aoba-ku, Sendai, 980-0845, Japan*
[c]*Advanced Institute for Materials Research (WPI-AIMR), Tohoku University, 2-1-1 Katahira, Aoba-ku, Sendai, 980-8577, Japan*

† Electronic supplementary information (ESI) available. See DOI: https://doi.org/10.1039/d4gc02006e

hydrogenation of alkene products (DODH + hydrogenation; DODH + HG). Our group developed ReO_x–Pd/CeO_2 [31,32] and ReO_x–Au/CeO_2 [33,34] catalysts as the first examples for DODH + HG and DODH, respectively. However, the high cost of Re, Pd and Au limits their industrial applicability. Very recently, our group has also developed the ReO_x–Ag/CeO_2 catalyst[35] and the ReO_x/CeO_2 + Ni/CeO_2 catalyst,[36] both of which do not require expensive additive metals of Au or Pd. However, these state-of-the-art catalysts are still expensive because of the requirement of Re as active species.

Owing to their potential to replace the costly Re species in the conventional DODH catalysts, Mo-based catalysts have been extensively investigated for DODH reactions, *e.g.*, dioxo-Mo(VI) complexes, molybdate salts and supported Mo catalysts.[16] The first developed Mo-based catalysts are dioxo-Mo(VI) complexes (the first paper was published in 2013 [37]). The Mo centers in the complex catalysts are typically coordinated with a bulky ligand to stabilize the Mo complex.[38–44] Non-green reductants such as PPh_3 and metallic Al were used in these studies. The reported yields by the Mo complex catalysts were not high in comparison with the systems using homogeneous Re catalysts with the same reductants. Molybdate salts like ammonium heptamolybdate (AHM), a typical commercially-available Mo compound, are also effective in DODH reactions. In 2014, only slightly later than the first report for the Mo complex catalysts for DODH, the use of AHM as a DODH catalyst was reported.[45] This report used diol as both a substrate and reductant. Yet, the product yield was not high (45% yield of 1-hexene from 1,2-hexanediol). Later studies also used AHM as the DODH catalyst in combination with various reductants such as 2-propanol[46] and Na_2SO_3,[47] and good yields from simple aliphatic diols were achieved with relatively inexpensive 2-propanol as the reductant (77% yield of 1-hexene). To enhance the reusability and stability, supported Mo catalysts were then investigated. In 2017, Palkovits *et al.* reported the first supported Mo-based DODH catalyst, MoO_x/TiO_2,[48,49] which achieved 55% yield of 2,5-dihydrofuran (2,5-DHF) from 1,4-anhydroerythritol (1,4-AHERY) using 3-octanol as a reducing agent. This catalyst was reusable at least 5 times. Meanwhile, the use of H_2 as a reductant with Mo-based DODH catalysts was not reported until our recent paper. In 2022, our group found the combination of MoO_x–Au/TiO_2 and H_2 to achieve 77% yield of 2,5-DHF from 1,4-AHERY.[50] The additive metal of Au played a crucial role in the activation of H_2, in a similar manner to the ReO_x–Au/CeO_2 catalyst. Almost at the same time, Pagán-Torres *et al.* reported the MoO_x–Pd/TiO_2 catalyst for the DODH + HG reaction using H_2 as a reductant.[51] Although high product yields were not pursued in this report, very high selectivity (>98%) to tetrahydrofuran (THF) from 1,4-AHERY was reported at the 1,4-AHERY conversion of 29%.

Although Mo-based DODH catalysts typically necessitate higher reaction temperatures than Re-based catalysts,[52,53] their abundance makes them more industrially attractive. Nonetheless, the widespread application of MoO_x–M/support (M = Au or Pd) catalysts still remains a challenge due to the high cost of noble additive metals. The role of Au and Pd is to activate H_2. In contrast, some non-noble metals, particularly first-row transition metals such as Fe, Ni, Co and Cu, are more accessible and commonly employed for hydrogenation of various organic compounds.[54–57] Ni and Cu are also generally used in methanol synthesis *via* CO hydrogenation.[58,59] In DODH reactions, Ni has been demonstrated to be a good co-catalyst for the activation of H_2 in the ReO_x/CeO_2 + Ni/CeO_2 system mentioned above.[36] Such effectiveness posits the potential of non-noble first-row transition metals as alternatives to Au to reduce catalyst costs. In this research, therefore, to decrease the cost of catalysts, the development of DODH catalysts consisting of only non-noble metals was targeted.

Experimental

Catalyst preparation

MoO_x–M/TiO_2 catalysts (M = Fe, Co, Ni, Cu, Ag or Pd) were prepared by the sequential impregnation (imp) method. First, 2 g of TiO_2 (anatase; Catalysis Society of Japan, JRC-TIO-7; BET surface area 270 m^2 g^{-1}) was added to a beaker placed on a heating plate. Then, an aqueous solution of each precursor (nitrate of M, whose amount corresponded to 2 wt% M (Fe, Co, Ni and Cu), 1 wt% Ag or 0.3 wt% Pd) was added to TiO_2 until the surface of TiO_2 was saturated (*i.e.*, incipient wetness method). The mixture was stirred well with a glass bar at 363 K until being completely dried. The process was repeated until all the precursor solution was consumed. The solid was dried at 383 K overnight in a drying oven and calcined at 773 K for 3 h with a heating rate of 10 K min^{-1} to give M/TiO_2. Next, MoO_x was loaded on M/TiO_2. An aqueous solution of 0.0184 g Mo precursor ($(NH_4)_6Mo_7O_{24}{\cdot}4H_2O$ (AHM); 10 mg Mo) was added to 1 g of M/TiO_2 with the same procedure as the impregnation of M. The catalysts (MoO_x–M/TiO_2) were used in the activity test after being dried at 383 K overnight in a drying oven without calcination. For the MoO_x–Cu–Na/TiO_2 catalysts, a mixed solution of AHM and $Na_2MoO_4{\cdot}2H_2O$ (typical amounts: 0.0166 g AHM and 0.0025 g $Na_2MoO_4{\cdot}2H_2O$; Mo : Na molar ratio = 100 : 15) was used for the loading of Mo species onto M/TiO_2. The loading amount of Mo was 1 wt% for both MoO_x–M/TiO_2 and MoO_x–Cu–Na/TiO_2 catalysts unless otherwise noted. The typical loading amount of Cu was 2 wt%. Catalysts with other loading amounts were also prepared by changing the precursor amount(s).

For preparing Au/TiO_2 and MoO_x–Au/TiO_2, Au species was loaded with the deposition–precipitation (dp) method.[50] The TiO_2 powder was dispersed in a $HAuCl_4{\cdot}4H_2O$ aqueous solution (Au content corresponded to 0.3 wt% of TiO_2) at 353 K. The pH of the solution was adjusted to 8 by the gradual addition of 0.1 M NH_3 aq. with constant stirring for 4 h. The suspension was filtered, and the recovered solid was washed several times with distilled water (2 L) at room temperature. After drying overnight at 383 K, Au/TiO_2 was calcined in air at 673 K for 4 h, for which the heating rate was controlled to be 1 K min^{-1}. The loading of Mo onto Au/TiO_2 was carried out in

the same way as that for the other MoO_x–M/TiO_2 catalysts (*vide supra*).

The control catalysts, ReO_x–^{dp}Au/CeO_2 (Re 1 wt%, Au/Re = 0.3), ReO_x–Ag/CeO_2 (Re 1 wt%, Ag/Re = 0.3) and ReO_x–Pd/CeO_2 (Re 2 wt%, Pd/Re = 0.25), were prepared by following the same procedure in our previous reports.[32,33,35]

Activity test

A 190 mL stainless–steel autoclave with a glass inner vessel was used as the reactor for activity tests. For the typical reaction, 0.15 g catalyst, 0.5 g substrate, 0.1 g internal standard (*n*-dodecane), 4.0 g solvent (1,2-dimethoxyethane (1,2-DME)) and a stirrer bar were added into the glass vessel. The glass vessel was set into the autoclave, and then, 1 MPa H_2 was used to purge the autoclave 3 times, followed by the pressurization with 5.1 MPa (8 MPa at 463 K) H_2. A heater was used to control the reaction temperature, and the inner temperature was monitored *via* a thermocouple. The time when the temperature reached the target one was defined as 0 h. After the reaction, the autoclave was rapidly cooled down to room temperature in a water bath. The gas phase was collected in a gas bag for the runs where gaseous products were generated. Afterwards, the inside of the autoclave was washed with 15 g of the washing solvent (the same liquid as the reaction solvent was employed). The resulting liquid was collected, combined and analyzed. The liquid and gaseous samples were analyzed by GC-FID with a TC-WAX column. For product identification, GC-MS was used in conjunction with commercially available authentic samples. Any undefined peaks in the GC charts were labeled as "others" in this study. In most conditions, the reaction results consistently showed a carbon balance of 100 ± 10%.

The conversion, selectivity, carbon balance and yield were calculated by using the following equations (eqn (1)–(4)), where *n* and *N*c represent the mole of each compound and the number of carbon atom in each compound, respectively.

$$\text{Conversion} = \frac{n(\text{input substrate}) - n(\text{unreacted substrate})}{n(\text{input substrate})} \times 100\% \quad (1)$$

$$\text{Selectivity} = \frac{n(\text{product}) \cdot Nc(\text{product})}{\sum n(\text{product}) \cdot Nc(\text{product})} \times 100\% \quad (2)$$

$$\text{Carbon balance} = \frac{n(\text{unreacted substrate}) \cdot Nc(\text{substrate}) + \sum n(\text{product}) \cdot Nc(\text{product})}{n(\text{input substrate}) \cdot Nc(\text{substrate})} \times 100\% \quad (3)$$

$$\text{Yield} = \frac{\text{conversion} \cdot \text{selectivity}}{100\%} \quad (4)$$

For the reuse experiments, the liquid phase and catalyst were separated *via* centrifugation at 6000 rpm for 10 min after the reaction. Afterwards, the catalyst was washed three times with 1,2-DME. The catalyst was then dried in a drying oven at the temperature of 383 K for 3 h. Optionally, the dried catalyst was further calcined at 573 K for 3 h with a heating rate of 10 K min^{-1}. After drying (+calcination), the catalyst was used for the next round of activity test.

Catalyst characterization

Thermogravimetry-differential thermal analysis (TG-DTA) was carried out with a Rigaku Thermo Plus EVO-II instrument. About 10 mg of sample was set on a Pt pan and heated in an air flow (30 mL min^{-1}) with a heating rate of 10 K min^{-1} from room temperature to 1173 K.

X-ray diffraction (XRD) patterns were acquired using a Rigaku MiniFlex600 diffractometer. Cu Kα radiation (λ = 0.154 nm) was employed as the X-ray source. Samples were measured at a scanning rate of 10° min^{-1} along the 2θ axis from 3° to 90°.

Analysis of scanning-transmission electron microscopy (STEM) was conducted with an FEI Titan^3 60–300 electron microscope equipped with a Super-X detector (Thermo Fisher Scientific) for energy-dispersive X-ray spectroscopy (EDX). Samples were dispersed in ethanol and ultrasonicated. After transferring the suspension onto a Cu or Pt grid, the grid was air-dried at ambient temperature until the complete evaporation of ethanol.

Temperature-programmed reduction with H_2 (H_2-TPR) was carried out with a fixed-bed flow-type reactor equipped with a thermal conductivity detector (TCD). The sample amount was 50 mg. Argon was used to dilute H_2 gas (5%), and the total flow rate of gas was 30 mL min^{-1}. The reactor was heated from room temperature to 1273 K with a heating rate of 10 K min^{-1}.

X-ray absorption spectroscopy (XAS) was conducted at the BL14B2 beamline of SPring-8 (proposal number: 2022B1746). The catalyst samples after the reaction were collected, dried and sealed in a plastic bag in a glove bag filled in N_2 to avoid the undesired sample exposure to air. Cu K-edge XAS data were acquired in a transmission mode. Mo K-edge XAS data were obtained in either a fluorescence or transmission mode. All the measurements were conducted at room temperature. The Demeter software package[60] was used to manage the XAS data. Athena software was used to subtract a linear function from the pre-edge region and normalize the data on the basis of the edge jump. The k^3-weighted $\chi(k)$ data were Fourier-transformed after the Hanning window function was applied. The Artemis software was used to fit the EXAFS oscillations to the Fourier-transformed data in *R*-space.

Results and discussion

Catalyst development

A series of additive metals (M) in MoO_x–M/TiO_2 catalysts were tested in the DODH reaction of 1,4-anhydroerythritol (1,4-AHERY) as a model substrate, and the results are summarized in Table 1. Note that 1,4-AHERY is a typical biomass-derived platform molecule that is used for DODH reactions due to its high reactivity.[61] The primary DODH product was 2,5-dihydrofuran (2,5-DHF), and typical byproducts were THF (hydrogenated product of 2,5-DHF), 2,3-dihydrofuran (2,3-DHF; isomer-

Table 1 Screening of additive metals (M) in the MoO_x–M/TiO_2 catalysts for DODH of 1,4-AHERY[a]

Entry	M	Conv. [%]	Selectivity [%]					Carbon balance [%]
			2,5-DHF	THF	2,3-DHF	1,4-BuD	Others	
1[b]	Au	35.0	99.9	0.0	0.0	0.0	0.1	100.6
2[c]	Pd	43.0	0.0	99.9	0.0	0.0	0.1	96.5
3	Ag	56.7	97.4	0.1	0.3	0.4	1.8	97.0
4	Cu	62.4	97.8	0.1	0.5	0.6	0.9	98.3
5	Fe	8.0	67.4	1.1	0.5	4.1	27.0	98.2
6	Co	4.1	84.4	2.0	0.6	5.0	8.1	92.2
7	Ni	9.3	75.1	2.1	1.9	8.0	12.9	100.6
8[d]	Cu	86.6	69.4	15.0	1.0	3.2	11.4	96.5
9[e]	None	4.1	81.3	4.7	1.9	1.6	10.5	103.5

DHF = dihydrofuran; BuD = butanediol. [a] Reaction conditions: 1,4-AHERY (0.5 g), 1,2-DME (4 g), *n*-dodecane (internal standard) (0.1 g), catalyst (Mo (1 wt%), M (2 wt%)) (0.15 g), H_2 (8 MPa) (initial pressure (5.1 MPa) at r.t.), 463 K, 4 h. [b] TiO_2 (P25) support, Au (0.3 wt%), Mo (1 wt%). [c] TiO_2 (P25) support, Pd (0.3 wt%), Mo (1 wt%). [d] 24 h reaction. [e] MoO_x/TiO_2, without M added.

ized product of 2,5-DHF) and 1,4-butanediol (1,4-BuD; over-reaction product of THF and dihydrofurans).[62] The formation of 1,4-BuD from 2,5-DHF resulted from the consecutive reaction consisting of isomerization to 2,3-DHF and hydration to 2-hydroxytetrahydrofuran and hydrogenation (Fig. S1†), as reported previously;[62] in this subsequent reaction, the isomerization step is the key, and the later steps proceed relatively easily. Carbon-supported ReO_x catalysts were reported to be effective for the isomerization of 2,5-DHF and even complete conversion to 1,4-BuD.[63]

Among the various additive metals (M) in the MoO_x–M/TiO_2 catalysts tested at 463 K for 4 h, Ag and Cu showed comparably high DODH activity (entries 3 and 4). The yield of DODH (or DODH + HG) product by these catalysts was higher than those by the MoO_x–^{dp}Au/TiO_2 (P25) and MoO_x–^{imp}Pd/TiO_2 (P25) (Au or Pd = 0.3 wt%, Mo = 1 wt%) catalysts, both of which were reported in our previous work (entries 1 and 2),[50] under the current reaction conditions. The higher yields provided here are attributable to the difference of TiO_2 supports (P25 for the current study *vs.* anatase for previous studies) in addition to the class of M. Given that Cu is more abundant and cheaper than Ag, we focused more on the Cu-based catalysts in the following investigation.

The extension of the reaction time with the MoO_x–Cu/TiO_2 catalyst enabled us to achieve high 1,4-AHERY conversion, while the yield of 2,5-DHF did not increase over 65% because of the formation of THF, 1,4-BuD and other unidentified compounds ("others") as by-products (entry 8 of Table 1 and Table S1†). The decrease of reaction temperature to 413 K suppressed the formation of "others", but the formation of 1,4-BuD instead became prominent at the high 1,4-AHERY conversion (Table S1†). The high yield of 2,5-DHF was thus not obtained over the MoO_x–Cu/TiO_2 catalysts.

DODH reaction itself does not require acidic or basic catalysts, while acidic species rather induces undesired side reactions. Based on this insight, a part of Mo precursor ($(NH_4)_6Mo_7O_{24}$; AHM) was replaced with a basic one (Na_2MoO_4) in the catalyst preparation in order to decrease the acidity of catalysts (the prepared catalysts are hereafter represented by MoO_x–Cu–Na/TiO_2). The selectivity to 2,5-DHF was successfully increased upon the partial replacement of acidic precursor (AHM) with the basic one (Na_2MoO_4) (Table S2†). However, too much Na rather decreased both the selectivity to 2,5-DHF and the activity of MoO_x–Cu–Na/TiO_2 catalysts. When only Na_2MoO_4 was used as the Mo precursor (Mo : Na = 100 : 200), almost no 2,5-DHF was obtained in the reaction for 16 h at 463 K. The activity of MoO_x–Cu–Na/TiO_2 catalysts was not changed much at the Na/Mo molar ratio of less than 1, while that was slightly decreased by the further increase of Na amount (Tables S2 and S3†). The highest selectivity to 2,5-DHF at 463 K was obtained at the Mo : Na ratio of 100 : 15, which was selected in the following study.

The time course of the DODH reaction of 1,4-AHERY at 463 K over the MoO_x–Cu–Na/TiO_2 (2 wt% Cu, 1 wt% Mo, Mo : Na = 100 : 15) is shown in Fig. 1 and Table S4.† The high 1,4-AHERY conversion was obtained even at 0 h (just after the inner temperature reached 463 K), indicating the high activity of the MoO_x–Cu–Na/TiO_2 catalyst. The selectivity to 2,5-DHF was almost 100% at the short reaction time and then slowly decreased until 24 h when the conversion of 1,4-AHERY reached about 90%. During the initial 24 h, the main by-product was THF, which was probably formed *via* the hydrogenation of 2,5-DHF. After 24 h, the formation of 1,4-BuD started, and the formation of THF was also accelerated. The highest yield of 2,5-DHF (81%) was observed at 24 h. This yield was higher than that obtained over MoO_x–^{dp}Au/TiO_2 (1 wt% Mo, 0.3 wt% Au, 77% yield) and those with homogeneous Mo catalysts (maximum 75% yield with the AHM catalyst and 2-propanol reductant)[50] but lower than that over ReO_x–^{dp}Au/CeO_2 (1 wt% Re, 0.3 wt% Au, 91% yield)[34] (Table S1†). The turnover number (TON) based on Mo atoms in the MoO_x–Cu–Na/TiO_2 catalyst reached 270, the value of which was also higher than those obtained with reported Mo-based DODH catalysts.

Next, the effect of the loading amounts of Mo and Cu in MoO_x–Cu–Na/TiO_2 was investigated (Fig. 2, 3 and S2, Tables S6 and S7†). In the dependence of activity on the Mo loading amount (Fig. 2), the volcano-type plot with steep slopes on

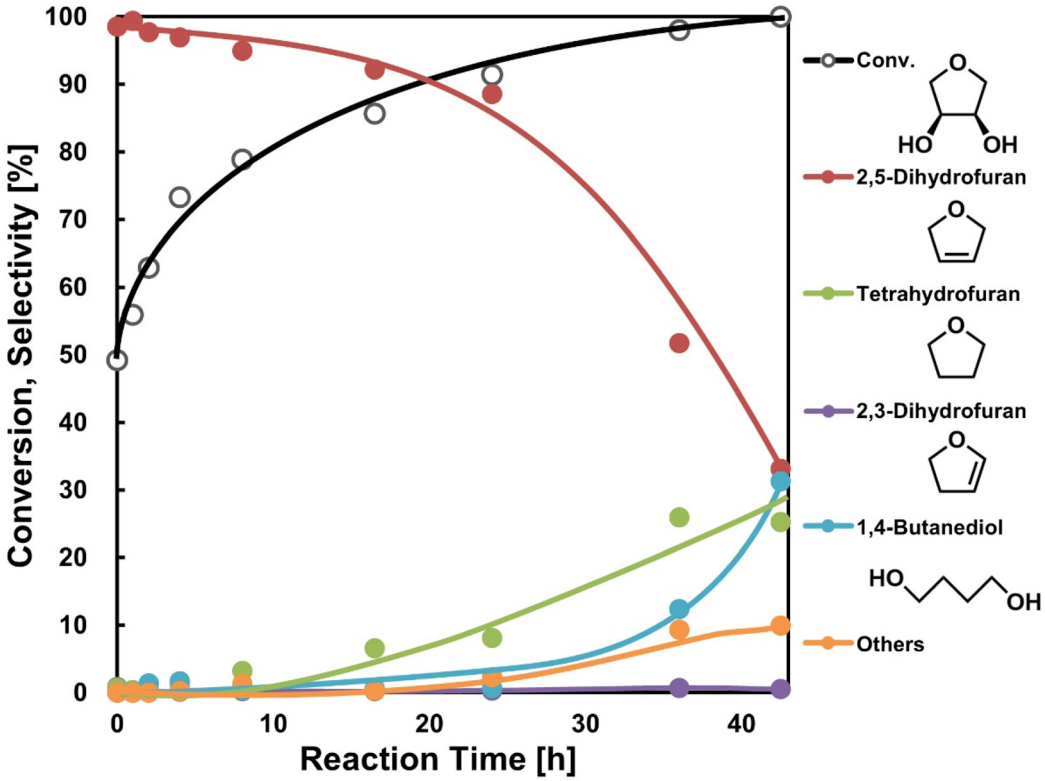

Fig. 1 Time course of DODH of 1,4-AHERY over the MoO_x–Cu–Na/TiO_2 catalyst. Reaction conditions: 1,4-AHERY (0.5 g), 1,2-DME (4 g), *n*-dodecane (internal standard) (0.1 g), MoO_x–Cu–Na/TiO_2 (2 wt% Cu, 1 wt% Mo, Mo : Na = 100 : 15) (0.15 g), H_2 (8 MPa) (initial pressure 5.1 MPa at r. t.), 463 K. The details are listed in Table S4.†

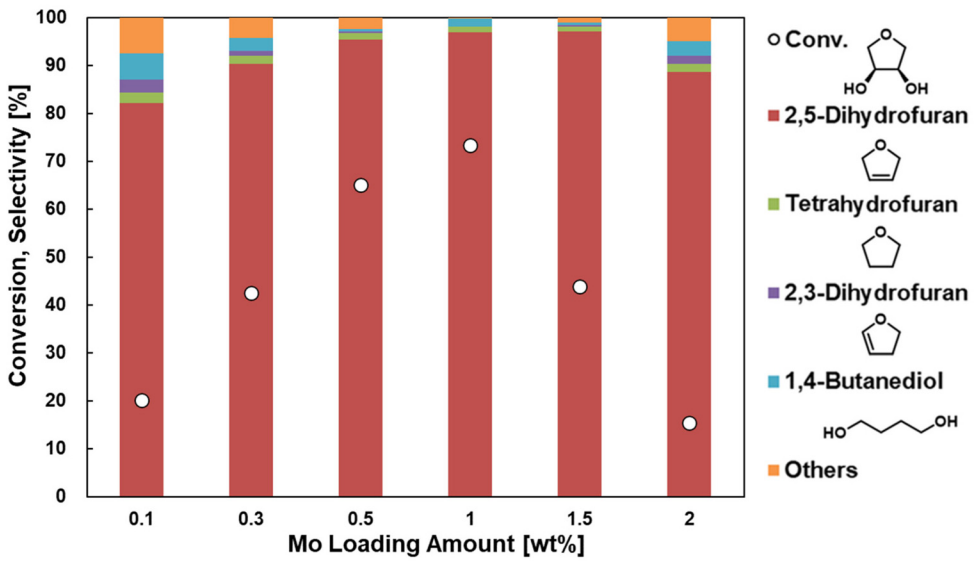

Fig. 2 Dependence of the DODH performance of MoO_x–Cu–Na/TiO_2 catalysts on the Mo loading amount. Reaction conditions: 1,4-AHERY (0.5 g); 1.2-DME (4 g), *n*-dodecane (internal standard) (0.1 g), MoO_x–Cu/TiO_2 (Cu 2 wt%, Mo : Na = 100 : 15) (0.15 g), H_2 (8 MPa) (initial pressure (5.1 MPa) at r.t.), 463 K, 4 h. The details are listed in Table S6.†

both sides was observed. The highest activity was provided at 1 wt% of Mo loading, while the selectivity to 2,5-DHF (DODH product) was high in the Mo-loading range from 0.1 wt% to 2 wt%. Thus, 1 wt% Mo was selected as the optimum Mo loading amount for the MoO_x–Cu–Na/TiO_2 catalysts. For the previously developed catalyst MoO_x–^{dp}Au/TiO_2,[50] the excess

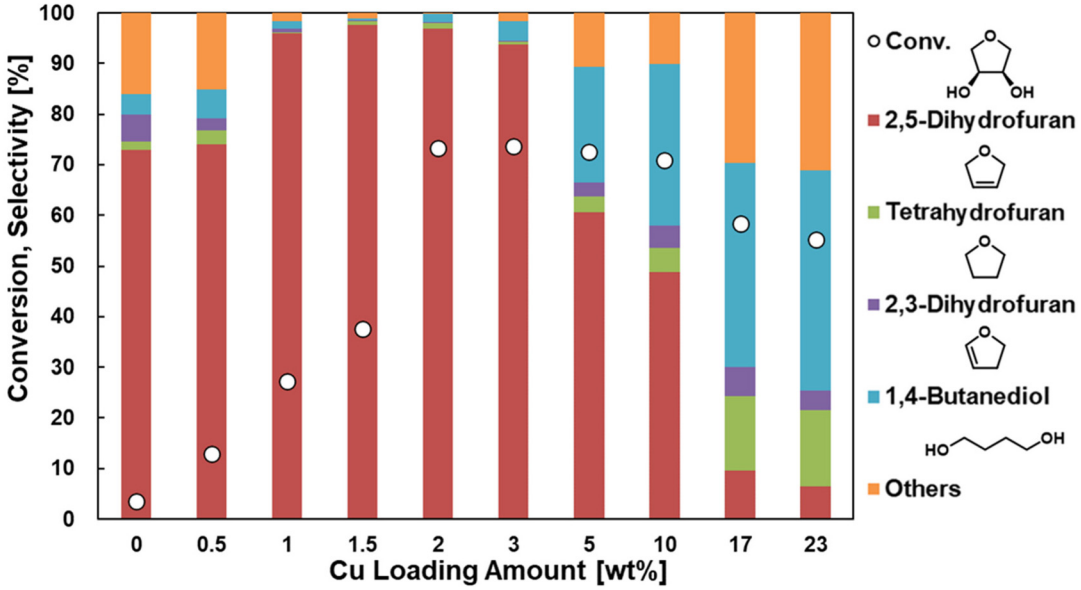

Fig. 3 Dependence of DODH performance of MoO_x–Cu–Na/TiO_2 catalysts on Cu loading amount. Reaction conditions: 1,4-AHERY 0.5 g; 1.2-DME 4 g, *n*-dodecane (internal standard) 0.1 g, MoO_x–Cu/TiO_2 (Mo 1 wt%, Mo : Na = 100 : 15) 0.15 g, H_2 8 MPa (initial pressure 5.1 MPa at r.t.), 463 K, 4 h. The details are listed in Table S7.†

loading of Mo did not decrease the activity. The difference between MoO_x–Cu–Na/TiO_2 and MoO_x–^{dp}Au/TiO_2 can be explained by the low reducibility of Cu species in MoO_x–Cu–Na/TiO_2 with high Mo loading. At a higher Mo loading amount, the reduction temperature of Cu got significantly increased (Fig. S8†). The details will be discussed in the characterization section (*vide infra*).

For the effect of Cu amount (Fig. 3), with the increase of Cu loading amount, the conversion and selectivity to 2,5-DHF were increased until 2 wt%. Over 2 wt%, the conversion and selectivity to 2,5-DHF got decreased due to the formation of by-products, mainly 1,4-BuD. For the Au-promoted catalyst MoO_x–^{dp}Au/TiO_2,[50] the activity was reported to be almost independent on the Au loading amount in the range of 0.1–0.6 wt%, and the selectivity to 2,5-DHF was also almost unchanged. The little dependence of the catalytic performance on the amount of promoter was also reported for ReO_x/CeO_2 catalysts (promoter: Pd, Ag and Ni).[32,35,36] The necessity of a larger amount of Cu compared to the other promoters can be explained by the larger particle size of Cu, which results in the lower number of Cu particles; the details of structural features will be discussed later. The reason for the formation of 1,4-BuD over the MoO_x–Cu–Na/TiO_2 catalysts with high Cu loadings (>5 wt%) was assumed to be the activity of Cu species for the conversion of 2,5-DHF. In fact, the formation of 1,4-BuD from 2,5-DHF was confirmed in the control reactions using 2,5-DHF as a substrate in the presence of either Cu/TiO_2 with a high Cu loading or CuO as a catalyst (Table S8†). After the reaction of 2,5-DHF operated under pressurized H_2, CuO was totally reduced to Cu metal, which was visibly obvious by the color of the spent catalyst and also confirmed by XRD (Fig. S2†). Cu metal phase was also found in Cu/TiO_2 (5 wt%) and Cu/TiO_2 (10 wt%) by XRD after their catalytic use for the reduction of 2,5-DHF. With the increase in the Cu loading amount, both the particle size and number of Cu particles increased, triggering the Cu-catalyzed formation of 1,4-BuD. Thus, 2 wt% was chosen to be the appropriate loading amount of Cu in MoO_x–Cu–Na/TiO_2.

Applicability of the MoO_x–Cu–Na/TiO_2 catalyst

The applicability of the MoO_x–Cu–Na/TiO_2 catalyst to other diols was examined (Table 2). As the compounds consisting of linear carbon backbone with terminal vicinal diol, 1,2-butanediol was converted to 1-butene in 32% yield (at 43% conversion; entry 1), and 1,2-pentanediol was transformed into 1-pentene in 52% yield (at 58% conversion; entry 2). The substrate with a longer carbon chain gave better selectivity. The main by-product was *n*-alkane generated *via* the hydrogenation of the target olefin. The similar yield of 1-pentene from 1,2-pentanediol was reported over MoO_x–^{dp}Au/TiO_2 under almost the same conditions,[50] while the reaction time was much shorter with the MoO_x–Cu–Na/TiO_2 catalyst (4 h for MoO_x–Cu–Na/TiO_2 *vs.* 24 h for MoO_x–^{dp}Au/TiO_2). This observed superiority of MoO_x–Cu–Na/TiO_2 is reflected by the higher promotion ability of Cu (with enough amount) than Au. Meanwhile, the selectivity to alkane (DODH + HG product) over MoO_x–Au/TiO_2 was <1%, which was lower than 9% given by MoO_x–Cu–Na/TiO_2. The progress of the reaction by lowering the substrate amount and prolonging the reaction time over MoO_x–Cu–Na/TiO_2 gave the intensive formation of the alkane product (entry 3).

For cyclic diols, *cis*-1,2-cyclohexanediol was converted to cyclohexene in 82% yield (entry 5), which was higher than the value obtained over the MoO_x–^{dp}Au/TiO_2 catalyst (66%).[50] The higher yield of cyclohexene by MoO_x–Cu–Na/TiO_2 originates

Table 2 DODH reaction of various diols over the MoO_x–Cu–Na/TiO_2 catalyst[a]

Entry	Substrate (amount [mmol])	Reaction time [h]	Conv. [%]	Product (selectivity [%])	Carbon balance [%]
1	1,2-Butanediol (5.55) 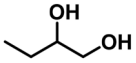	4	43.2	1-Butene (74.0), *n*-butane (26.0), others (<0.1)	99.0
2	1,2-Pentanediol (4.80) 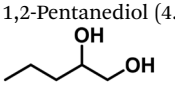	4	58.3	1-Pentene (90.4), *n*-pentane (9.1), others (0.5)	99.1
3[b]	1,2-Pentanediol (2.40)	8	84.8	1-Pentene (54.7), *n*-pentane (38.9), others (6.4)	99.4
4[b]	*cis*-1,2-Cyclohexanediol (2.15) 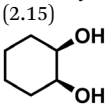	4	75.2	Cyclohexene (96.0), cyclohexane (0.0), *trans*-isomer (1.5), others (2.5)	94.5
5[b]	*cis*-1,2-Cyclohexanediol (2.15)	16	93.3	Cyclohexene (87.8), cyclohexane (5.3), *trans*-isomer (0.8), others (6.0)	100.7
6[b]	*trans*-1,2-Cyclohexanediol (2.15) 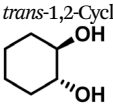	4	9.1	Cyclohexene (57.7), cyclohexane (0.0), *cis*-isomer (28.3), others (14.0)	98.5
7[c]	Styrene glycol (1.81) 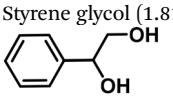	1	89.3	Styrene (42.7), ethylbenzene (53.6), phenethyl alcohol (3.6), others (<0.1)	84.0
8	Diethyl L-tartrate (2.42) 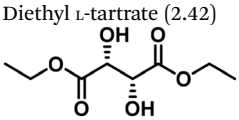	4	62.6	Diethyl fumarate (69.3), diethyl succinate (21.4), diethyl maleate (1.4), others (7.9)	96.5
9[b]	Diethyl L-tartrate (1.21)	8	>99.9	Diethyl fumarate (4.0), diethyl succinate (67.7), diethyl maleate (0), others (28.3)	92.2

[a] Reaction conditions: substrate (0.5 g), 1,2-DME (4 g), *n*-dodecane (internal standard) (0.1 g), MoO_x–Cu–Na/TiO_2 catalyst (1.0 wt% Mo, 2.0 wt% Cu, Mo : Na = 100 : 15) (0.15 g), H_2 (8 MPa) (initial pressure (5.1 MPa) at r.t.), 463 K. [b] Substrate (0.25 g). [c] Styrene glycol (0.25 g), catalyst (0.3 g), hydroquinone (0.05 g) as a polymerization inhibitor, *n*-dodecane (internal standard) (0.1 g), H_2 (4 MPa) (initial pressure (2.9 MPa) at r.t.), 413 K.

from the low reactivity of cyclohexene for hydrogenation and also low activity of MoO_x–Cu–Na/TiO_2 for dehydration. The MoO_x–Au/TiO_2 catalyst proceeded with the formation of cyclohexanol and cyclohexanone (7.6% selectivity to these compounds at 73% conversion of *cis*-1,2-cyclohexanediol), while the formation of these monooxygenates was negligible over MoO_x–Cu–Na/TiO_2. The removal of acid sites by the addition of Na in MoO_x–Cu–Na/TiO_2 could be responsible for suppressing the formation of monooxygenates. The reactivity of *trans*-1,2-cyclohexanediol was much lower than that of the *cis*-isomer (entry 6), whose behavior is quite common in DODH systems.[32,34,50] The formation of the *cis*-isomer was found in the reaction of *trans*-1,2-cyclohexanediol. Cyclohexene was produced probably *via* the isomerization to *cis*-1,2-cyclohexanediol and subsequent DODH.

Styrene glycol showed significantly different reactivity from the other substrates (entry 7, Tables 2 and S8†). Under the standard reaction conditions (463 K, substrate/catalyst = 0.5 g/0.15 g), the styrene glycol was completely converted even during the heating to 463 K (*i.e.*, reaction time = 0 h), and the main product was ethylbenzene (DODH + HG product). However, the carbon balance was only 54%. A possible reason for this poor carbon balance is the formation of polystyrene because styrene is known to readily undergo the polymerization at high temperature.[64] The addition of a typical polymerization inhibitor, hydroquinone,[65] slightly improved the carbon balance by *ca.* 12% (Table S9†). However, by TG-DTA (Fig. S3†), the weight loss of the solid after the reaction without hydroquinone was only 5.0 wt% (corresponding to 1.6% of the charged substrate), which was much less than the loss of carbon balance (46% loss of carbon balance as polystyrene (corresponding to 53 wt% weight loss in TG)). Soluble styrene oligomers were assumed to be generated; such species have a wide range of molecular weight due to different numbers of monomeric units involved, and thus, were unable to be detected by GC-FID. Therefore, the milder reaction conditions (lower reaction temperature and H_2 pressure) were applied in order to suppress the formation of ethylbenzene and polystyrene. Under the conditions of 363 K and 4 MPa H_2, the carbon balance was successfully kept at >90% with the

conversion level of *ca.* 80% (16 h); however, the main product was still ethylbenzene. Also, when 0.5 wt% Cu catalyst was employed (Table S10†), the conversion was significantly low. Compared with the standard 2.0 wt% Cu catalyst, the difference in the conversion level was much larger than that in the reaction of 1,4-AHERY (Fig. 3, Table S7†). The significant decrease in the conversion with the 0.5 wt% Cu catalyst was probably due to the blockage of Cu sites by polystyrene; that is, even if the formation amount of polystyrene was limited, the small number of Cu sites underwent the coverage by polystyrene easily. To increase the yield of styrene over MoO_x–Cu–Na/TiO_2, the moderate reaction temperature (413 K) and short reaction time were used to suppress the hydrogenation reaction of the produced styrene, and hydroquinone was added as a polymerization inhibitor. As a result, styrene was obtained in 38% yield (entry 7, Table 2). This value is similar to the highest styrene yield in DODH of styrene glycol with H_2 ever reported with the ReO_x–C catalyst (39%).[66]

Other heterogeneous DODH or DODH + HG catalysts were also tested in the reaction of styrene glycol (Table S10†). MoO_x–Au/TiO_2, MoO_x–Ag/TiO_2, ReO_x–Au/CeO_2 and ReO_x–Ag/CeO_2 catalysts, all of which are effective for DODH (not DODH + HG), showed good selectivity to styrene; however, the conversion level (<15%) was much lower than that over MoO_x–Cu–Na/TiO_2. On the other hand, ReO_x–Pd/CeO_2, which is an effective DODH + HG catalyst, completely converted styrene glycol to ethylbenzene. Ideally, the activities of ReO_x–M/CeO_2 catalysts are similar because the rate-determining step of DODH reaction is the extrusion of alkene from the reduced Re diolate species regardless of M species. The high conversion over ReO_x–Pd/CeO_2 means that the intrinsic reactivity of styrene glycol is very high. The C=C bond in a styrene molecule is conjugated with the phenyl group, while such conjugation is absent in styrene glycol. The stabilization by conjugation may lead to the high reactivity of styrene glycol toward DODH. The lower conversions obtained over ReO_x–Au/CeO_2 and ReO_x–Ag/CeO_2 than that over ReO_x–Pd/CeO_2 could be due to the blockage of active sites on the former two catalysts by polystyrene and also the inhibition of polystyrene formation on the latter Pd-modified catalyst by rapid hydrogenation of the produced styrene. Similarly, for the Mo-based catalysts, the Au- and Ag-modified catalysts were significantly deactivated because of the formation of polystyrene.

For the reaction of diethyl L-tartrate (entries 8 and 9, Table 2), the converted substrate amount was comparable to those of 1,2-alkanediols. The hydrogenation of the DODH product (diethyl fumarate) to diethyl succinate proceeded readily, and the obtained yield of diethyl fumarate was at most 43%. The increase of conversion by decreasing the substrate amount and prolonging the reaction time rather decreased the yield of diethyl fumarate because of its subsequent hydrogenation. The production of succinic acid from tartaric acid in good yield has been reported with MoO_x–M/TiO_2 catalysts (M: noble metal).[67] Effective catalytic systems for the DODH of tartaric acid or tartrates to the olefinic products with H_2 as a reductant have not yet been reported. Our previously reported Re/CeO_2-based catalysts were also tested for the reaction of diethyl L-tartrate (Table S11†); however, the conversion was much lower than that of polyols (the considerable conversion required much higher temperature such as 463 K), and diethyl fumarate or diethyl succinate was hardly formed. The TG-DTA results of ReO_x–^{dp}Au/CeO_2 and ReO_x–Pd/CeO_2 catalysts after the reaction of diethyl L-tartrate at 463 K are shown in Fig. S4.† The exothermic weight losses of 14.9% and 13.8% were observed at around 473 K for ReO_x–^{dp}Au/CeO_2 and ReO_x–Pd/CeO_2, respectively, which were about 16 equivalents of the substrate molecule to Re and corresponded to about 8% conversion. These results suggest that the low carbon balance was due to the intensive adsorption of organic molecules onto the catalyst surfaces as well as formation of products that cannot be detected by GC. Considering that there are several Re-based catalysts that are effective for DODH of sugar acids and their esters,[68–72] the CeO_2 support seems to be inappropriate for the substrates containing carboxyl group(s) or carboxylate. MoO_x/TiO_2-based catalysts are more suitable to this type of substrate.

Additionally, the performance of the MoO_x–Cu–Na/TiO_2 catalyst in alcohol solvents (2-propanol and ethanol) was investigated with 1,4-AHERY as a substrate, because alcohol solvents have higher dissolution ability for highly functionalized biomass-related molecules. As shown in Table S12,† the catalyst exhibited similarly high activity in these alcohol solvents to the case of 1,2-dimethoxyethane (1,2-DME), yet the selectivity to 2,5-DHF became slightly lower. These results demonstrated the applicability of the MoO_x–Cu–Na/TiO_2 catalyst to not only ether solvents but also alcohol solvents, positing the great potential of this catalyst in the conversion of more functionalized biomass-derived molecules.

Reusability of the MoO_x–Cu–Na/TiO_2 catalyst

The reusability of MoO_x–Cu–Na/TiO_2 was evaluated in the DODH reaction of 1,4-AHERY. The activity and selectivity to 2,5-DHF (DODH product) from 1,4-AHERY showed no significant differences in four-times reuse, where the catalysts were dried and calcined at 573 K for 3 h before each run (Fig. 4(A)). However, the activity (conversion of 1,4-AHERY) was significantly decreased when the catalysts were only dried after each run (Fig. 4(B)). The good stability of regenerated (calcined before reuse run) catalyst and low stability without regeneration were also reported for the MoO_x–^{dp}Au/TiO_2 catalyst;[50] however, the MoO_x–^{dp}Au/TiO_2 catalyst showed a slight decrease in the selectivity to 2,5-DHF and a gradual increase in the selectivity to 1,4-BuD. In this context, the MoO_x–Cu–Na/TiO_2 catalyst was concluded as a more stable catalyst for the DODH reaction of 1,4-AHERY, compared to MoO_x–^{dp}Au/TiO_2.

The TG-DTA profiles for the spent MoO_x–Cu–Na/TiO_2 catalysts and as-prepared one are shown in Fig. S5.† The as-prepared catalyst (A) only showed a small loss of weight (0.4%) at around 513 K, which is mainly attributed to the combustion of ammonium ions derived from the Mo precursor (AHM). The spent catalysts (B–E) showed a significant exothermic signal with a loss of weight at around 490 K, which is assignable to the combustion of surface-deposited organic species. The com-

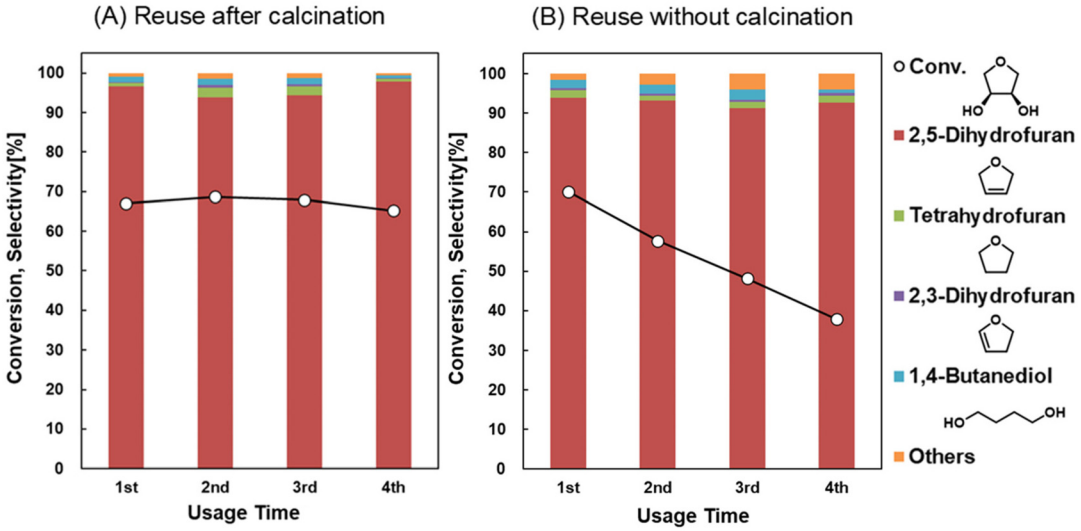

Fig. 4 Reuse experiments of MoO_x–Cu–Na/TiO_2 catalysts in DODH of 1,4-AHERY with different treatment procedure: (A) reused after calcination at 573 K for 3 h; (B) reused only after drying overnight at 383 K. Reaction conditions: 1,4-AHERY 0.5 g, 1.2-DME 4 g, *n*-dodecane (internal standard) 0.1 g, MoO_x–Cu–Na/TiO_2 (2 wt% Cu, 1 wt% Mo, Mo : Na = 100 : 15) 0.15 g, H_2 8 MPa (initial pressure 5.1 MPa at r.t.), 463 K, 4 h.

busted amount in the catalyst after the 1st use was 4.0 wt%, which corresponds to about 4 equivalents of 1,4-AHERY to Mo. A larger amount of organic compounds than Mo diolate was thus adsorbed or deposited. The combusted amount was gradually increased to 5.5 wt% upon the repeated use. The increase of adsorbed or deposited carbonaceous species could be the reason for the gradual deactivation of the MoO_x–Cu–Na/TiO_2 catalyst. Thus, the good reusability of calcined catalysts results from the removal of such organic species. For MoO_x–^{dp}Au/TiO_2 after the reaction (1,4-AHERY, 463 K, 1,2-DME solvent, a similar turnover number),[50] a similar combustion signal was observed (peak temperature: 510 K) with a lower weight loss (2.9% weight loss around the exothermic peak), in addition to the coke combustion (1.6% weight loss around the exothermic peak at 736 K). The MoO_x–Cu–Na/TiO_2 catalyst produces almost the same amount of total organic deposited species as the case of MoO_x–^{dp}Au/TiO_2, but the coke amount was lower. The lower amount of coke which cannot be removed by the regeneration (calcination at 573 K) could lead to the higher selectivity to 2,5-DHF over the regenerated MoO_x–Cu–Na/TiO_2 catalysts than regenerated MoO_x–^{dp}Au/TiO_2 for four-times reuse (98% *vs.* 90%).[50]

Kinetic study on the DODH reaction of 1,4-AHERY over the MoO_x–Cu–Na/TiO_2 catalyst

The effects of H_2 pressure and substrate amount on the DODH reaction of 1,4-AHERY over the MoO_x–Cu–Na/TiO_2 catalyst are shown in Fig. 5 and 6 (their detailed data are summarized in Tables S13 and S14,† respectively). The reaction order with respect to the H_2 pressure was 0.13 in the range from 2 MPa to 8 MPa (Fig. 5). This small reaction order suggests that the steps in which H_2 participates are fast, including the reduction of catalyst (copper oxide to copper metal). Similar little dependence on the H_2 pressure has been also observed in the case of MoO_x–^{dp}Au/TiO_2. The reaction order with respect to the concentration of the substrate (1,4-AHERY) was 0.10 (Fig. 6). The small reaction order suggests that the adsorption of the substrate onto the catalyst surfaces is fast and saturated. Based on the generally accepted mechanism of DODH and the currently observed kinetics, the reaction proceeds *via* the fast reduction of MoO_x species, fast adsorption of the substrate to form Mo diolate intermediates, and extrusion of the olefinic product from the Mo diolate. The extrusion of the olefinic product is the rate-determining step. This mechanism is similar to the proposed ones for MoO_x–Au/TiO_2 and ReO_x–M/CeO_2 (M = Pd, Au, Ag) catalysts.[32,34,35,50]

Catalyst characterization

The MoO_x–Cu/TiO_2 catalysts were characterized by X-ray diffraction (XRD), scanning-transmission electron microscopy with energy-dispersive X-ray spectroscopy (STEM-EDX), temperature-programmed reduction with H_2 (H_2-TPR) and X-ray absorption spectroscopy (XAS).

The XRD patterns of the MoO_x–Cu–Na/TiO_2 catalysts after their catalytic use (Fig. S6†) did not show any peaks related to Mo species or Cu species regardless of the Cu amounts except for the case of the sample with a high Cu loading (5 wt%). The absence of MoO_x peaks has been also reported for MoO_x–^{dp}Au/TiO_2 catalysts with the same Mo loading amount, which was due to the low Mo amount and high dispersion of Mo species.[50] The absence of XRD peaks of 0.5–3 wt% Cu metal suggests the high dispersion of Cu species; however, the different possibilities of low crystallinity and/or low reduction degree of Cu species cannot be ruled out. In the XRD pattern of the catalysts with 5 wt% Cu, the peaks assignable to the fcc Cu metal, which was formed by the reduction of Cu species in the as-prepared catalyst under

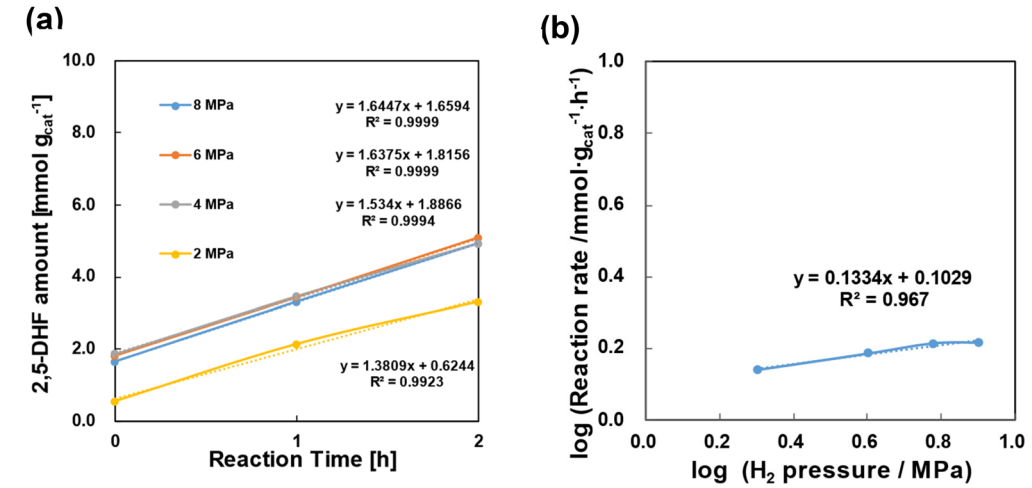

Fig. 5 Dependence of the initial reaction rate over the MoO_x–Cu–Na/TiO_2 catalyst on H_2 pressure. (a) Raw data. (b) Double logarithmic plot of the reaction rate as a function of H_2 pressure. Reaction rate (mmol (g_{cat} h)$^{-1}$) = $yield_{2,5\text{-DHF}}$ (mmol)/(reaction time (h) × catalyst amount (g)). Reaction conditions: 1,4-AHERY (0.5 g), 1,2-DME (4 g), *n*-dodecane (internal standard) (0.1 g), MoO_x–Cu–Na/TiO_2 (1 wt% Mo, 2 wt% Cu, Mo : Na = 100 : 15) (0.15 g), H_2 (2–8 MPa), 423 K, 0–2 h. The details are listed in Table S13.†

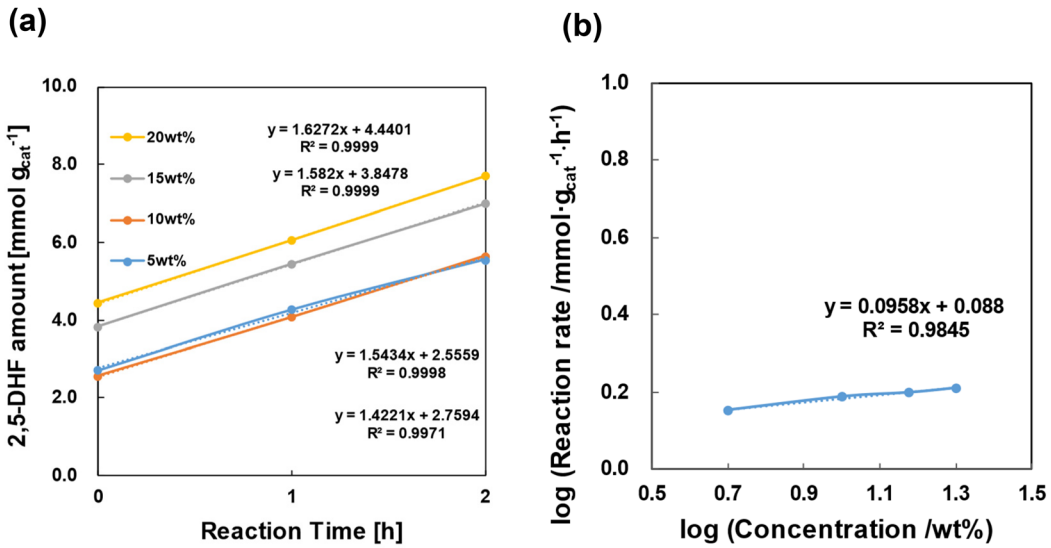

Fig. 6 Dependence of the initial reaction rate over the MoO_x–Cu–Na/TiO_2 catalyst on the substrate concentration. (a) Raw data. (b) Double logarithmic plot of the reaction rate as a function of the substrate concentration. Reaction rate (mmol (g_{cat} h)$^{-1}$) = $yield_{2,5\text{-DHF}}$ (mmol)/(reaction time (h) × catalyst amount (g)). Reaction conditions: 1,4-AHERY 0.5 g, 1,2-DME 2–9.5 g, *n*-dodecane (internal standard) (0.1 g) MoO_x–Cu–Na/TiO_2 (1.0 wt% Mo, 2.0 wt% Cu, Mo : Na = 100 : 15) (0.15 g), H_2 (8 MPa), 423 K, 0–2 h. The details are listed in Table S14.†

the reaction conditions, were observed. The particle size of Cu in the 5 wt% Cu catalyst was calculated from XRD to be 18 nm.

The STEM-EDX images of the MoO_x–Cu–Na/TiO_2 catalysts are shown in Fig. 7 and S7.† The Mo species were distributed uniformly in all the catalysts, agreeing with the XRD results. The uniform distribution of Mo species has also been reported for MoO_x–Au/TiO_2.[50] The Cu species were present as particles with *ca.* 20 nm in diameter. In the catalyst with 1 wt% Cu, the spherical Cu particles were sparsely present. The lower activity of 1 wt% Cu catalyst could be due to the too small number of Cu particles by their aggregation; the portions in the absence of Cu particles do not have activity. The number of Cu particles was larger in the Cu 2 wt% catalyst without a significant change of the particle size of Cu species. On the other hand, in the Cu 5 wt% catalyst, the shape of Cu particles became block-like, and Cu species were also widely distributed on the support. Considering the XRD results, these Cu particles in the 5 wt% Cu catalyst were fcc Cu^0 crystals. The structural change can be related to the selectivity change found in Fig. 2.

In the H_2-TPR profiles (Fig. S9†), MoO_x/TiO_2 showed a reduction signal between 673 and 773 K with a peak

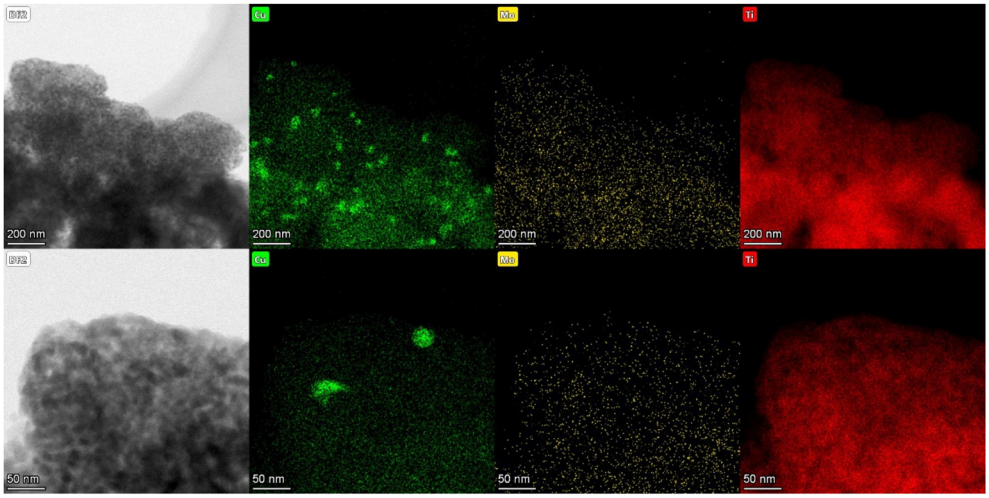

Fig. 7 STEM-EDX images of MoO_x–Cu–Na/TiO_2 (1 wt% Mo, 2 wt% Cu, Mo : Na = 100 : 15), after the reaction (4 h in Fig. 1).

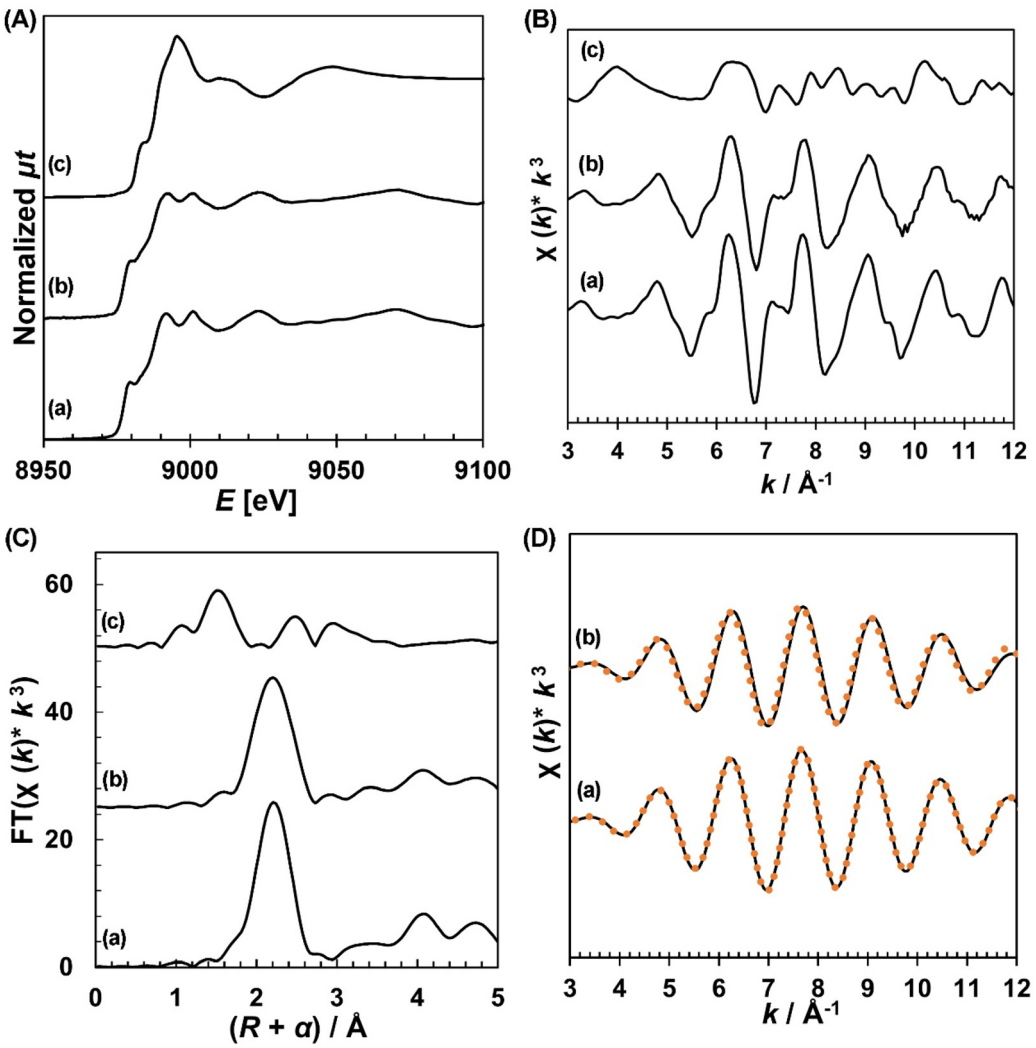

Fig. 8 (A) Cu K-edge XANES spectra of catalysts and standard compounds. (B) k^3-Weighted EXAFS oscillations shown in the k-space. (C) k^3-Weighted EXAFS oscillations shown in the R-space; the data were not phase-corrected. (D) Filtered spectra (solid lines) and fitting (dotted lines). Fourier-filtering range is listed in Table S15.† (a) Cu foil, (b) MoO_x–Cu–Na/TiO_2 (2 wt% Cu, 1 wt% Mo, Mo : Na = 100 : 15) after the reaction for 4 h, (c) CuO.

maximum at 725 K. The H_2 consumption amount calculated from this signal was 0.27 mmol g^{-1}, which was about 3 equivalents to the Mo amount (1 wt% Mo = 0.10 mmol-Mo g^{-1}). Considering that the complete reduction of MoO_3 to Mo metal with H_2 is difficult, both MoO_3 and surface TiO_2 were reduced at the same time. The simultaneous reduction of MoO_3 and TiO_2 support was also reported for MoO_x/TiO_2 (P-25);[50] however, the current MoO_x/TiO_2 (anatase) showed the smaller total H_2 consumption amount and higher starting temperature of the reduction than the reported MoO_x/TiO_2 (P-25) catalyst. The anatase TiO_2 support in MoO_x/TiO_2 seems more difficult to be reduced than the rutile TiO_2 support. The addition of Cu species to MoO_x/TiO_2 drastically shifted the reduction signal toward the low-temperature side. In the case of MoO_x–Cu/TiO_2, no peak appeared at around 725 K, and a peak at 481 K was observed. Although the peak-top temperature (481 K) was higher than the standard reaction temperature (463 K), the reduction started below 463 K. For MoO_x–Ni/TiO_2, MoO_x–Co/TiO_2 and MoO_x–Fe/TiO_2, the reduction did not begin below 593 K. The difficulty in the reduction of MoO_x species could be related to the low catalytic activity (Table 1). For MoO_x–Ag/TiO_2 with the similar activity to MoO_x–Cu(–Na)/TiO_2, the main reduction signal was located at a similarly high temperature to those of MoO_x–Ni/TiO_2 and MoO_x–Fe/TiO_2, while the weak reduction signal was present at around the standard reaction temperature of 463 K. Both Cu and Ag can promote the

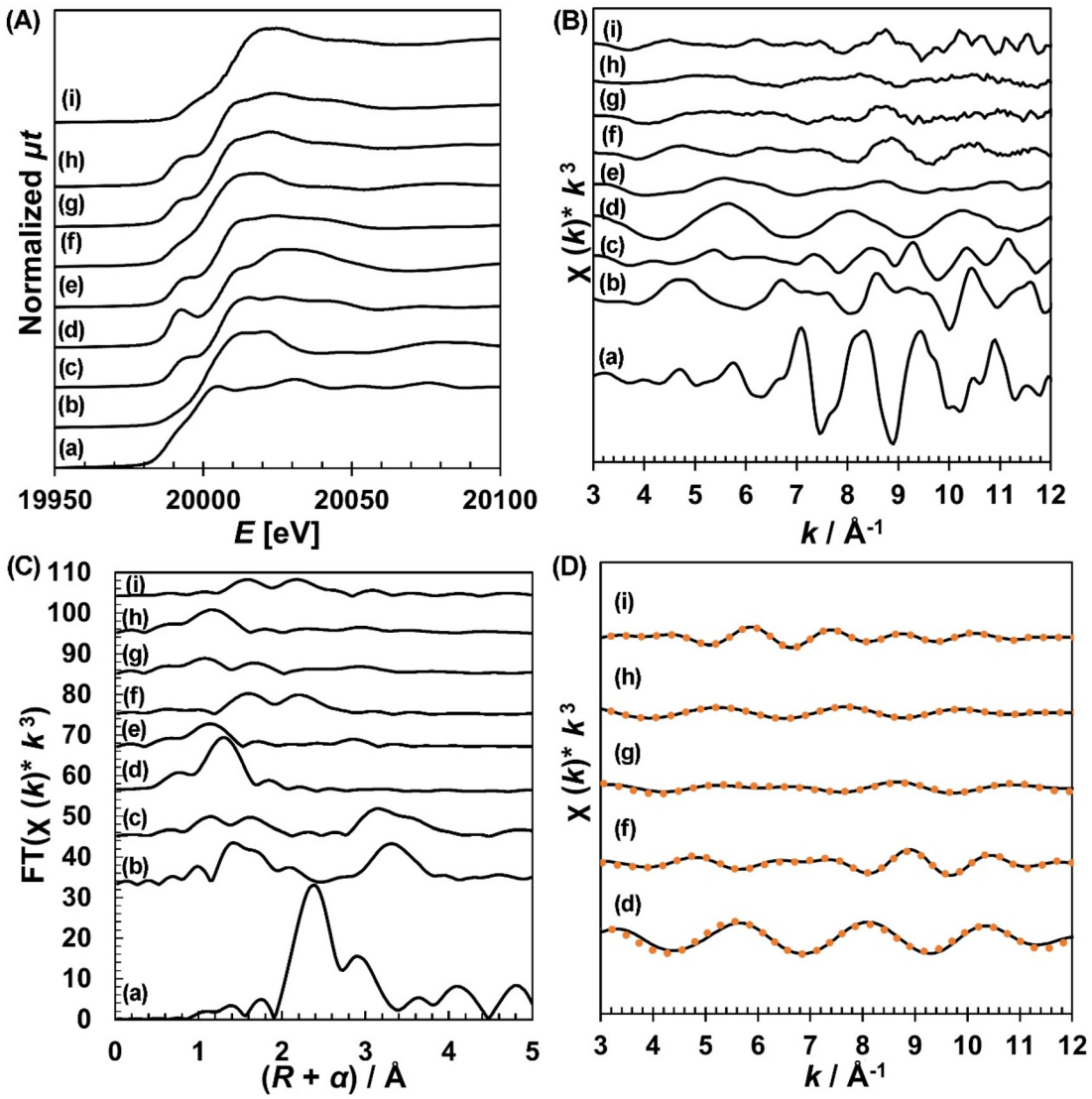

Fig. 9 (A) Mo K-edge XANES spectra of catalysts and standard compounds. (B) k^3-Weighted EXAFS oscillations shown in the k-space. (C) k^3-Weighted EXAFS oscillations shown in the R-space, the data were not phase-corrected. (D) Filtered spectra (solid lines) and fitting (dotted lines). Fourier-filtering range is listed in Table S16.† (a) Mo foil, (b) MoO_2, (c) MoO_3, (d) Na_2MoO_4, (e) $(NH_4)_6Mo_7O_{24}{\cdot}4H_2O$ (AHM), (f) MoO_x–Cu–Na/TiO_2 (2 wt% Cu, 1 wt% Mo, Mo : Na = 100 : 15) after use for 4 h, (g) MoO_x–Na/TiO_2 (1.0 wt% Mo, Mo : Na = 100 : 15) after use for 4 h, (h) MoO_x–^{dp}Au/TiO_2 (P-25 support, Au 0.3 wt%, Mo 1 wt%) before the reaction; (i) MoO_x–^{dp}Au/TiO_2 (P-25 support, Au 0.3 wt%, Mo 1 wt%) after use for 24 h. The data of (h), (i) and standard compounds have been reported.[50]

reduction of MoO_x species. The H_2-TPR profiles for MoO_x–Cu–Na/TiO_2 with the different Mo : Na molar ratios are also shown in Fig. S9.† The addition of Na only slightly shifted the reduction peak by *ca.* 10 K. This observation suggests that the reduction of Mo with H_2 was not affected by the Na additive. These results agreed with that the activity of MoO_x–Cu–Na/TiO_2 was almost independent on the Na amount (Table S2†). Based on the H_2-TPR data of the catalysts with the different Mo : Na ratios, we assumed that the Na^+ ion did not interact with MoO_x and rather basically bound on the TiO_2 support surface. The H_2-TPR profiles for the MoO_x–Cu–Na/TiO_2 catalysts (Mo : Na = 100 : 15) with the different Mo loading amounts are shown in Fig. S8.† Cu/TiO_2 and MoO_x–Cu–Na/TiO_2 with Mo 0.5 wt% and Cu 1 wt% showed similar profiles with the reduction signal at around 473 K, and the first peaks (293 K–540 K) exhibited higher H_2 consumption than that required for CuO reduction, which suggested that Mo, Cu and a part of surface Ti species were simultaneously reduced. The reduction is suggested to proceed well at the reaction temperature of 463 K. However, when the Mo loading amount increased over 1 wt%, the reduction signal of Cu was significantly shifted toward the high-temperature side. For the MoO_x–Cu–Na/TiO_2 catalyst with the Mo loading amount of 2 wt%, the peak of reduction temperature appeared at 553 K, and the reduction did not start below 463 K. The reduction of Cu species was thus suppressed by the excess amount of Mo, and this behavior is related to the low activity of MoO_x–Cu–Na/TiO_2 catalysts with the high Mo loadings (Fig. S9†).

The results of Cu K-edge X-ray absorption near-edge structure (XANES) and extended X-ray absorption fine structure (EXAFS) in both *k*-space and *R*-space are shown in Fig. 8. The XANES spectrum of MoO_x–Cu–Na/TiO_2 after its catalytic use was similar to that of Cu^0 foil. The EXAFS spectrum of the same catalyst can be fitted well with the Cu–Cu metal bond with a coordination number (CN) of 10.7 (Table S15†). These results agreed well with the STEM-EDX results where the Cu species were present as relatively large metallic particles.

The Mo K-edge XANES and EXAFS data are shown in Fig. 9. The XANES spectrum of MoO_x–Cu–Na/TiO_2 after the reaction (f) was similar to those of MoO_2 (b) and MoO_x–Au/TiO_2 after the reaction (i). The EXAFS spectrum and curve-fitting result (Table S16†) of MoO_x–Cu–Na/TiO_2 after the reaction (f) were also similar to those of MoO_x–Au/TiO_2 after the reaction (i). The results demonstrate that the structure of Mo species in MoO_x–Cu–Na/TiO_2 during the reaction was similar to that in MoO_x–Au/TiO_2 where Mo^{IV} oxide cluster species are dominant.[50] A recent DFT study of MoO_x species on TiO_2 surfaces also suggests that the dimeric Mo species are good active sites for DODH when H_2 is sufficiently activated.[73] On the other hand, Cu-free MoO_x–Na/TiO_2 after the reaction (g) provided a similar spectrum to that of MoO_3 (c). Although the structure was different from MoO_x–Au/TiO_2 before the reaction where AHM-like Mo K-edge EXAFS spectrum was obtained ((h) and (e)),[50] the valence of Mo was +6, demonstrating that Cu species promoted the reduction of Mo species like Au.

Conclusions

MoO_x–Cu/TiO_2 catalysts exhibited a good performance in the DODH reaction of various diols. The use of a small amount of the basic Mo precursor Na_2MoO_4 (MoO_x–Cu–Na/TiO_2) enhanced the selectivity to DODH products, achieving the highest yield of 2,5-dihydrofuran (2,5-DHF) at 81% from 1,4-anhydroerythritol (1,4-AHERY). The Cu loading amount much affects the performance of MoO_x–Cu–Na/TiO_2: the loading amount less than 2 wt% decreased the activity and that above 3 wt% much decreased the selectivity to the target product. In comparison with a more expensive MoO_x–Au/TiO_2 catalyst, a higher yield and higher initial rate were obtained by MoO_x–Cu–Na/TiO_2. This catalyst maintained its performance through at least three reuse cycles without significant drops in the conversion or selectivity when the spent catalyst was calcined before each run. The MoO_x–Cu–Na/TiO_2 catalyst displayed broad substrate scope including both linear and cyclic diols. Notably, this catalyst also worked well for tartaric ester, which is difficult to be converted to the corresponding DODH product in the reported catalysts with H_2 as the reductant. The kinetic study with the MoO_x–Cu–Na/TiO_2 catalyst revealed that the release of the alkene is the rate-determining step, which is consistent with the general DODH mechanism with a sufficient supply of the reductant. Through various characterization studies, it was observed that Cu existed as metallic particles in the optimized catalyst (Cu 2 wt%, Mo 1 wt%), while Mo^{VI} was present on the surface of the catalyst. The Mo active site underwent the transition from the original oxidation state of +6 to +4 upon the activation of H_2 facilitated by Cu, in a similar way to MoO_x–M/TiO_2 (M: noble metal) catalysts.

Conflicts of interest

There are no conflicts to declare.

Acknowledgements

This work was supported by KAKENHI 23H05404, 23K20034 and 23K26451. J. G. appreciates the support from the "Amano Institute of Technology Scholarship" and "Global Hagi Scholarship". The authors also appreciate the assistance in STEM-EDS measurement by Mr Yuichiro Hayasaka (The Electron Microscopy Center, Tohoku University).

References

1 A. Corma, S. Iborra and A. Velty, *Chem. Rev.*, 2007, **107**, 2411–2502.
2 J. J. Bozell and G. R. Petersen, *Green Chem.*, 2010, **12**, 539–554.
3 M. J. Climent, A. Corma and S. Iborra, *Green Chem.*, 2011, **13**, 520–540.

4 M. Besson, P. Gallezot and C. Pinel, *Chem. Rev.*, 2014, **114**, 1827–1870.
5 B. M. Stadler, C. Wulf, T. Werner, S. Tin and J. G. de Vries, *ACS Catal.*, 2019, **9**, 8012–8067.
6 T. A. Ewing, N. Nouse, M. van Lint, J. van Haveren, J. Hugenholtz and D. S. van Es, *Green Chem.*, 2022, **24**, 6373–6405.
7 K. Tomishige, Y. Nakagawa and M. Tamura, *Green Chem.*, 2017, **19**, 2876–2924.
8 K. Tomishige, M. Yabushita, J. Cao and Y. Nakagawa, *Green Chem.*, 2022, **24**, 5652–5690.
9 Y. Nakagawa, M. Yabushita and K. Tomishige, *RSC Sustainability*, 2023, **1**, 814–837.
10 K. Avasthi, A. Bohre, M. Grilc, B. Likozar and B. Saha, *Catal. Sci. Technol.*, 2020, **10**, 5411–5437.
11 D. J. Ward, D. J. Saccomando, G. Walker and S. M. Mansell, *Catal. Sci. Technol.*, 2023, **13**, 2638–2647.
12 C. Boucher-Jacobs and K. M. Nicholas, in *Selective Catalysis for Renewable Feedstocks and Chemicals*, ed. K. M. Nicholas, 2014, vol. 353, pp. 163–184.
13 N. N. Tshibalonza and J.-C. M. Monbaliu, *Green Chem.*, 2020, **22**, 4801–4848.
14 F. C. Jentoft, *Catal. Sci. Technol.*, 2022, **12**, 6308–6358.
15 S. Raju, J. T. Jastrzebski, M. Lutz, L. O. Witteman, J. R. Dethlefsen, P. Fristrup, M.-E. Moret and R. J. K. Gebbink, *Inorg. Chem.*, 2015, **54**, 11031–11036.
16 A. R. Petersen and P. Fristrup, *Chem. – Eur. J.*, 2017, **23**, 10235–10243.
17 J. R. Dethlefsen and P. Fristrup, *ChemSusChem*, 2015, **8**, 767–775.
18 G. K. Cook and M. A. Andrews, *J. Am. Chem. Soc.*, 1996, **118**, 9448–9449.
19 B. Wozniak, Y. Li, S. Tin and J. G. de Vries, *Green Chem.*, 2018, **20**, 4433–4437.
20 I. Ahmad, G. Chapman and K. M. Nicholas, *Organometallics*, 2011, **30**, 2810–2818.
21 J. Yi, S. Liu and M. M. Abu-Omar, *ChemSusChem*, 2012, **5**, 1401–1404.
22 E. Arceo, J. A. Ellman and R. G. Bergman, *J. Am. Chem. Soc.*, 2010, **132**, 11408–11409.
23 M. Shiramizu and F. D. Toste, *Angew. Chem., Int. Ed.*, 2012, **51**, 8082–8086.
24 G. W. Huber and A. Corma, *Angew. Chem., Int. Ed.*, 2007, **46**, 7184–7201.
25 S. Kim, E. E. Kwon, Y. T. Kim, S. Jung, H. J. Kim, G. W. Huber and J. Lee, *Green Chem.*, 2019, **21**, 3715–3743.
26 X. Yao, T. J. Strathmann, Y. Li, L. E. Cronmiller, H. Ma and J. Zhang, *Green Chem.*, 2021, **23**, 1114–1129.
27 Y. S. Yun, C. E. Berdugo-Díaz and D. W. Flaherty, *ACS Catal.*, 2021, **11**, 11193–11232.
28 M. Žula, M. Grilc and B. Likozar, *Chem. Eng. J.*, 2022, **444**, 136564.
29 V. Canale, L. Tonucci, M. Bressan and N. d'Alessandro, *Catal. Sci. Technol.*, 2014, **4**, 3697–3704.
30 J. E. Ziegler, M. J. Zdilla, A. J. Evans and M. M. Abu-Omar, *Inorg. Chem.*, 2009, **48**, 9998–10000.
31 N. Ota, M. Tamura, Y. Nakagawa, K. Okumura and K. Tomishige, *Angew. Chem., Int. Ed.*, 2015, **54**, 1897–1900.
32 N. Ota, M. Tamura, Y. Nakagawa, K. Okumura and K. Tomishige, *ACS Catal.*, 2016, **6**, 3213–3226.
33 S. Tazawa, N. Ota, M. Tamura, Y. Nakagawa, K. Okumura and K. Tomishige, *ACS Catal.*, 2016, **6**, 6393–6397.
34 Y. Nakagawa, S. Tazawa, T. Wang, M. Tamura, N. Hiyoshi, K. Okumura and K. Tomishige, *ACS Catal.*, 2018, **8**, 584–595.
35 K. Yamaguchi, J. Cao, M. Betchaku, Y. Nakagawa, M. Tamura, A. Nakayama, M. Yabushita and K. Tomishige, *ChemSusChem*, 2022, e202102663.
36 K. Yamaguchi, Y. Nakagawa, C. Li, M. Yabushita and K. Tomishige, *ACS Catal.*, 2022, **12**, 12582–12595.
37 L. Hills, R. Moyano, F. Montilla, A. Pastor, A. Galindo, E. Álvarez, F. Marchetti and C. Pettinari, *Eur. J. Inorg. Chem.*, 2013, **2013**, 3352–3361.
38 K. Beckerle, A. Sauer, T. P. Spaniol and J. Okuda, *Polyhedron*, 2016, **116**, 105–110.
39 M. Stalpaert and D. De Vos, *ACS Sustainable Chem. Eng.*, 2018, **6**, 12197–12204.
40 R. Tran and S. M. Kilyanek, *Dalton Trans.*, 2019, **48**, 16304–16311.
41 J. Li, M. Lutz and R. Gebbink, *ChemCatChem*, 2020, **12**, 6356–6365.
42 R. Tran, C. A. Canote and S. M. Kilyanek, *Organometallics*, 2023, **42**, 1190–1197.
43 N. Wagner, W.-C. Tang, J. Wagner, B. Nguyen, J. Y. Lam, S. Gibbons-Stovall, A. Matias, S. Martinez, T. Trieu-Tran, G. Clabaugh, C. Navarro, I. Abboud, F. Flores, K. M. Nicholas and A. John, *Catal. Sci. Technol.*, 2024, DOI: **10.1039/D4CY00441H**.
44 R. S. Srivastava, *J. Organomet. Chem.*, 2024, **1003**, 122942.
45 J. R. Dethlefsen, D. Lupp, B. C. Oh and P. Fristrup, *ChemSusChem*, 2014, **7**, 425–428.
46 J. R. Dethlefsen, D. Lupp, A. Teshome, L. B. Nielsen and P. Fristrup, *ACS Catal.*, 2015, **5**, 3638–3647.
47 C. A. Navarro and A. John, *Inorg. Chem. Commun.*, 2019, **99**, 145–148.
48 L. Sandbrink, K. Beckerle, I. Meiners, R. Liffmann, K. Rahimi, J. Okuda and R. Palkovits, *ChemSusChem*, 2017, **10**, 1375–1379.
49 J. Sebastian, C. Mebrahtu and R. Palkovits, *Catal. Sci. Technol.*, 2023, **13**, 1087–1097.
50 S. Hacatrjan, L. Liu, J. Gan, Y. Nakagawa, J. Cao, M. Yabushita, M. Tamura and K. Tomishige, *Catal. Sci. Technol.*, 2022, **12**, 2146–2161.
51 S. Albarracin-Suazo, L. Freitas de Lima e Freitas, B. MacQueen, A. Heyden, J. A. Lauterbach, E. Nikolla and Y. J. Pagán-Torres, *ACS Sustainable Chem. Eng.*, 2022, **10**, 5719–5727.
52 B. E. Sharkey, A. L. Denning, F. C. Jentoft, R. Gangadhara, T. V. Gopaladasu and K. M. Nicholas, *Catal. Today*, 2018, **310**, 86–93.

53 Y. Xi, J. Lauterbach, Y. Pagan-Torres and A. Heyden, *Catal. Sci. Technol.*, 2020, **10**, 3731–3738.
54 M. H. Li, S. Y. Chen, Q. K. Jiang, Q. L. Chen, X. Wang, Y. Yan, J. Liu, C. C. Lv, W. P. Ding and X. F. Guo, *ACS Catal.*, 2021, **11**, 3026–3039.
55 G. A. Filonenko, R. van Putten, E. J. M. Hensen and E. A. Pidko, *Chem. Soc. Rev.*, 2018, **47**, 1459–1483.
56 G. Kyriakou, M. B. Boucher, A. D. Jewell, E. A. Lewis, T. J. Lawton, A. E. Baber, H. L. Tierney, M. Flytzani-Stephanopoulos and E. C. H. Sykes, *Science*, 2012, **335**, 1209–1212.
57 S. De, J. G. Zhang, R. Luque and N. Yan, *Energy Environ. Sci.*, 2016, **9**, 3314–3347.
58 M. Behrens, F. Studt, I. Kasatkin, S. Kuhl, M. Havecker, F. Abild-Pedersen, S. Zander, F. Girgsdies, P. Kurr, B. L. Kniep, M. Tovar, R. W. Fischer, J. K. Norskov and R. Schlogl, *Science*, 2012, **336**, 893–897.
59 F. Cannizzaro, E. J. M. Hensen and I. A. W. Filot, *ACS Catal.*, 2023, **13**, 1875–1892.
60 B. Ravel and M. Newville, *J. Synchrotron Radiat.*, 2005, **12**, 537–541.
61 Y. Nakagawa, T. Kasumi, J. Ogihara, M. Tamura, T. Arai and K. Tomishige, *ACS Omega*, 2020, **5**, 2520–2530.
62 T. Wang, S. Liu, M. Tamura, Y. Nakagawa, N. Hiyoshi and K. Tomishige, *Green Chem.*, 2018, **20**, 2547–2557.
63 T. Wang, M. Tamura, Y. Nakagawa and K. Tomishige, *ChemSusChem*, 2019, **12**, 3615–3626.
64 W. I. Bengough and G. B. Park, *Eur. Polym. J.*, 1978, **14**, 889–894.
65 F. Bovey and I. Kolthoff, *Chem. Rev.*, 1948, **42**, 491–525.
66 A. L. Denning, H. Dang, Z. Liu, K. M. Nicholas and F. C. Jentoft, *ChemCatChem*, 2013, **5**, 3567–3570.
67 A. Nacy, L. F. de Lima e Freitas, S. Albarracín-Suazo, G. Ruiz-Valentín, C. A. Roberts, E. Nikolla and Y. J. Pagán-Torres, *ChemCatChem*, 2021, **13**, 1294–1298.
68 M. Shiramizu and F. D. Toste, *Angew. Chem., Int. Ed.*, 2013, **52**, 12905–12909.
69 X. Li, D. Wu, T. Lu, G. Yi, H. Su and Y. Zhang, *Angew. Chem., Int. Ed.*, 2014, **53**, 4200–4204.
70 W. Deng, L. Yan, B. Wang, Q. Zhang, H. Song, S. Wang, Q. Zhang and Y. Wang, *Angew. Chem., Int. Ed.*, 2021, **60**, 4712–4719.
71 J. H. Jang, J. T. Hopper, I. Ro, P. Christopher and M. M. Abu-Omar, *Catal. Sci. Technol.*, 2023, **13**, 714–725.
72 X. Luo, R. Lu, H. Jiang, X. Si, J. Xu and F. Lu, *Ind. Eng. Chem. Res.*, 2021, **60**, 4510–4515.
73 D. Asada, T. Ikeda, K. Muraoka, Y. Nakagawa, K. Tomishige and A. Nakayama, *J. Phys. Chem. C*, 2022, **126**, 20375–20387.